Competing orders and the doping and momentum dependent quasiparticle excitations in cuprate superconductors ⋆

A.D. Beyer, C.-T. Chen, M.S. Grinolds, M.L. Teague, N.-C. Yeh *

Department of Physics, California Institute of Technology, Pasadena, CA 91125

Abstract

The low-energy quasiparticle excitations in hole- and electron-type cuprate superconductors are investigated via both experimental and theoretical means. It is found that the doping and momentum dependence of the empirical low-energy quasiparticle excitations is consistent with a scenario of coexisting competing orders and superconductivity in the ground state of the cuprates. This finding, based on zero-field quasiparticle spectra, is further corrobarated by the spatially resolved vortex-state scanning tunneling spectroscopy, which reveals pseudogap-like features consistent with a remaining competing order inside the vortex core upon the suppression of superconductivity. The competing orders compatible with empirical observations include the charge-density wave and spin-density wave. In contrast, spectral characteristics derived from incorporating the d-density wave as a competing order appear unfavorable in comparison with experiments.

Key words: cuprate superconductivity, competing orders, pseudogap, quasiparticle excitations
PACS: 74.50.+r, 74.62.Dh, 74.72.-h

1 Introduction

The physical origin of the pseudogap (PG) phenomena [1] and the apparent differences in the low-energy excitations of the hole- and electron-type

⋆ Work supported by the National Science Foundation through Grants #DMR-0405088.

* Corresponding author.
Email address: ncyeh@caltech.edu (N.-C. Yeh).

cuprates [2–6] are important and unresolved issues in high-temperature superconductivity. Empirically, the PG phenomena occur at two different energy scales [1]. One energy scale is a high-energy PG existent in both electron- and hole-type cuprates [7–10]. The other energy scale is a low-energy PG coexisting with superconductivity (SC) at low temperatures, which survives above the superconducting transition T_c and is manifested by the suppressed quasiparticle density of states (DOS) [2,3]. This PG has only been observed in hole-type cuprates and is found to correlate with the onset of the Nernst effect [1,11,12]. Our recent studies of the quasiparticle spectral density function and the DOS of various optimally doped cuprates [13] have revealed that the occurrence (absence) of the low-energy PG in hole- (electron-) type cuprate superconductors and the dichotomy in quasiparticle coherence [9,14] can be quantitatively understood as the result of a ground state consisting of coexisting competing orders (COs) and SC [15,16,18–22] with the presence of finite quantum fluctuations [6,23,24]. The objective of this work is to expand on our previous work [13] to further investigate how the coexistence of COs and SC may influence the doping and momentum dependence of the low-energy quasiparticle excitations in different cuprates. Specifically, we compare empirical quasiparticle spectra obtained from scanning tunneling spectroscopy and ARPES (angle-resolved photoemission spectroscopy) data in zero field with calculated quasiparticle DOS and spectral density functions. We focus on three COs: the charge-density wave (CDW) [16], spin-density wave (SDW) [17–19], and d-density wave (DDW) [1,20]. In addition, we perform spatially resolved quasiparticle tunneling spectra on both hole- and electron-type cuprates in the vortex state to investigate whether the spectral characteristics inside a vortex core are consistent with the presence of additional orders upon the suppression of SC. We find that the vortex-core states of both types of cuprates exhibit PG-like spectra, which differ from either the broad zero-bias bound states or flat conductance inside of the vortex core of conventional superconductors [25]. These finite-field results may be attributed to a remaining CO upon the suppression of SC, and are therefore corroborative of the notion of coexisting COs and SC in the cuprates.

2 Theoretical modeling

To investigate the effect of coexisting COs and SC on the low-energy excitations, we incorporate both COs and SC in the mean-field Hamiltonian $\mathcal{H}_{MF}$ and further include the quantum phase fluctuations associated with the coexisting CO and SC phases in the proper self-energy [13]. Specifically, we first obtain the bare Green's function $G_0(\mathbf{k},\omega)$ associated with a mean-field

Hamiltonian $\mathcal{H}_{MF} = \mathcal{H}_{\rm SC} + \mathcal{H}_{\rm CO}$, where

$$\mathcal{H}_{\rm SC} = \sum_{\mathbf{k},\sigma} \xi_{\mathbf{k}} c^{\dagger}_{\mathbf{k},\sigma} c_{\mathbf{k},\sigma} - \sum_{\mathbf{k}} \Delta_{\rm SC}(\mathbf{k}) (c^{\dagger}_{\mathbf{k},\uparrow} c^{\dagger}_{-\mathbf{k},\downarrow} + c_{-\mathbf{k},\downarrow} c_{\mathbf{k},\uparrow}) \tag{1}$$

is the superconducting Hamiltonian for a given pairing potential $\Delta_{\rm SC}(\mathbf{k})$, $\xi_{\mathbf{k}}$ is the normal-state eigenenergy, and $\sigma = \uparrow, \downarrow$ refers to the spin states. The mean-field CO Hamiltonian $\mathcal{H}_{\rm CO}$ with an energy scale $V_{\rm CO}$ and a wave-vector $\mathbf{Q}_1$ for CDW, $\mathbf{Q}_2$ for disorder-pinned SDW and $\mathbf{Q}_3$ for DDW can be expressed as follows [13]:

$$\begin{aligned}
\mathcal{H}_{\rm CDW} &= \sum_{\mathbf{k},\sigma} V_{\rm CDW} \left(c^{\dagger}_{\mathbf{k},\sigma} c_{\mathbf{k}+\mathbf{Q}_1,\sigma} + c^{\dagger}_{\mathbf{k}+\mathbf{Q}_1,\sigma} c_{\mathbf{k},\sigma} \right) \\
\mathcal{H}^{\rm pinned}_{\rm SDW} &= g^2 \sum_{\mathbf{k},\sigma} V_{\rm SDW} \left(c^{\dagger}_{\mathbf{k},\sigma} c_{\mathbf{k}+\mathbf{Q}_2,\sigma} + c^{\dagger}_{\mathbf{k}+\mathbf{Q}_2,\sigma} c_{\mathbf{k},\sigma} \right) \\
\mathcal{H}_{\rm DDW} &= \sum_{\mathbf{k},\sigma} V_{\rm DDW} \left(\cos k_x - \cos k_y \right) \left(i c^{\dagger}_{\mathbf{k}+\mathbf{Q}_3,\sigma} c_{\mathbf{k},\sigma} + h.c. \right),
\end{aligned} \tag{2}$$

where the coefficient g in $\mathcal{H}^{\rm pinned}_{\rm SDW}$ represents the coupling strength between disorder and SDW [19], $\mathbf{Q}_1$ is along the CuO_2 bonding direction $(\pi, 0)$ or $(0, \pi)$, $\mathbf{Q}_2 = \mathbf{Q}_1/2$, and $\mathbf{Q}_3$ is along (π, π) [20]. Here we have assumed that the density waves are static because dynamic density waves can be pinned by disorder, and in the latter case the momentum $\mathbf{k}$ remains a good quantum number as long as the mean free path is much longer than the superconducting coherence length, a condition generally satisfied in the cuprates at low temperatures. We have also neglected the direct coupling of antiferromagnetic SDW to SC [17] in the Hamiltonian because the corresponding phase space contribution of the first-order SDW coupling to the DOS is too small in the doped superconducting cuprates, similar to the situation of negligible DDW coupling to the DOS in the doped cuprates, to be elaborated in the next section. We further note that the spectroscopic characteristics associated with either CDW or disorder-pinned SDW as the CO are similar in the charge sector, although the wave-vector of CDW is twice of that of SDW [19].

To incorporate quantum phase fluctuations, we introduce a proper self-energy Σ^* in the zero-temperature zero-field limit. In this limit the longitudinal phase fluctuations dominate so that we can approximate Σ^* by the longitudinal part of the one-loop velocity-velocity correlation Σ^*_ℓ [26,27]:

$$\Sigma^*_\ell (\mathbf{k}, \omega) = \sum_{\mathbf{q}} \left[m \mathbf{v}_g(\mathbf{k}) \cdot \hat{\mathbf{q}} \right]^2 C_\ell(\mathbf{q}) G (\mathbf{k} - \mathbf{q}, \omega), \tag{3}$$

where the group velocity $\mathbf{v}_g$ is given by $\mathbf{v}_g = (\partial\xi_{\mathbf{k}}/\partial k)/\hbar$ for $|\mathbf{k}| \sim k_F$, and $C_\ell(\mathbf{q})$ is a coefficient that measures the degree of quantum fluctuations as detailed in Refs. [13,26,27], $\mathbf{q}$ is the momentum of quantum phase fluctuations, and $\xi_{\mathbf{k}}$ is given by realistic bandstructures [13]. Given $G_0(\mathbf{k},\omega)$ and $\Sigma^*_\ell(\mathbf{k},\omega)$ in (4×4) matrices with the basis $(c^\dagger_{\mathbf{k}\uparrow}\ c_{-\mathbf{k}\downarrow}\ c^\dagger_{\mathbf{k}+\mathbf{Q}\uparrow}\ c_{-(\mathbf{k}+\mathbf{Q})\downarrow})$, we can derive the full Green's function $G(\mathbf{k},\tilde{\omega})$ through the Dyson's equation [13]:

$$G^{-1}(\mathbf{k},\tilde{\omega}) = G_0^{-1}(\mathbf{k},\omega) - \Sigma^*_\ell(\mathbf{k},\tilde{\omega}), \tag{4}$$

where $\tilde{\omega} = \tilde{\omega}(\mathbf{k},\omega)$ denotes the energy renormalized by the phase fluctuations [13,26]. The Dyson's equation in Eq. (4) can be solved self-consistently [13] by first using the mean-field values of $\xi_{\mathbf{k}}$ and $\Delta_{\rm SC}$ and choosing an energy ω, then going over the momentum $\mathbf{k}$-values in the Brillouin zone by summing over a finite phase space in $\mathbf{q}$ near each $\mathbf{k}$, and finishing by finding the corresponding fluctuation renormalized quantities $\tilde{\xi}_{\mathbf{k}}$, $\tilde{\omega}$ and $\tilde{\Delta}_{\rm SC}$ until the solution to the full Green's function $G(\mathbf{k},\tilde{\omega})$ converges with an iteration method [13]. The converged Green's function yields the spectral density function $A(\mathbf{k},\omega) \equiv -{\rm Im}\left[{\rm G}(\mathbf{k},\tilde{\omega}(\mathbf{k},\omega))\right]/\pi$ and the DOS $\mathcal{N}(\omega) \equiv \sum_{\mathbf{k}} A(\mathbf{k},\omega)$.

3 Comparison with empirical data of quasiparticle excitations

Using the aforementioned approach, we find that many important features in the quasiparticle DOS of both hole- and electron-type cuprates of varying doping levels can be well described by a set of parameters $(\Delta_{\rm SC}, V_{\rm CO}, \eta, \mathbf{Q})$, where η denotes the magnitude of the quantum phase fluctuations [13,26,27] and is proportional to the mean-value of $C_\ell(\mathbf{q})$ in Eq. (3) by the relation $\langle C_\ell(\mathbf{q})\rangle = (2\hbar q/m_e)^2\eta$, with m_e being the electron mass. More specifically, we find that in the event of $V_{\rm CO} > \Delta_{\rm SC}$ and $T = 0$, there are two sets of spectral peak features at $\omega = \pm\Delta_{\rm SC}$ and $\omega = \pm\Delta_{\rm eff}$, with the effective excitation gap defined as $\Delta_{\rm eff} \equiv (\Delta^2_{\rm SC} + V^2_{\rm CO})^{1/2}$ [13]. The relative spectral weight of the peak features is largely determined by $\mathbf{Q}$, whereas the magnitude of the zero-bias conductance is sensitive to η [13]. Moreover, the zero-temperature features at $\omega = \pm\Delta_{\rm SC}$ begin to diminish in the spectral weight and shift to a smaller absolute energy with increasing temperature, and completely vanish above T_c. In contrast, the features at $\omega = \pm\Delta_{\rm eff}$ evolve with temperature into rounded "humps" at $\omega \sim \pm V_{\rm CO}$ for $T >\sim T_c$ [13], resulting in the well known low-energy pseudogap (PG) phenomena in optimally doped and underdoped hole-type cuprates. On the other hand, if $V_{\rm CO} < \Delta_{\rm SC}$, only one set of zero-temperature spectral peak features can be resolved at $\omega = \pm\Delta_{\rm eff}$, so that no PG is observed above T_c, which is consistent with the general findings in electron-type cuprates [13].

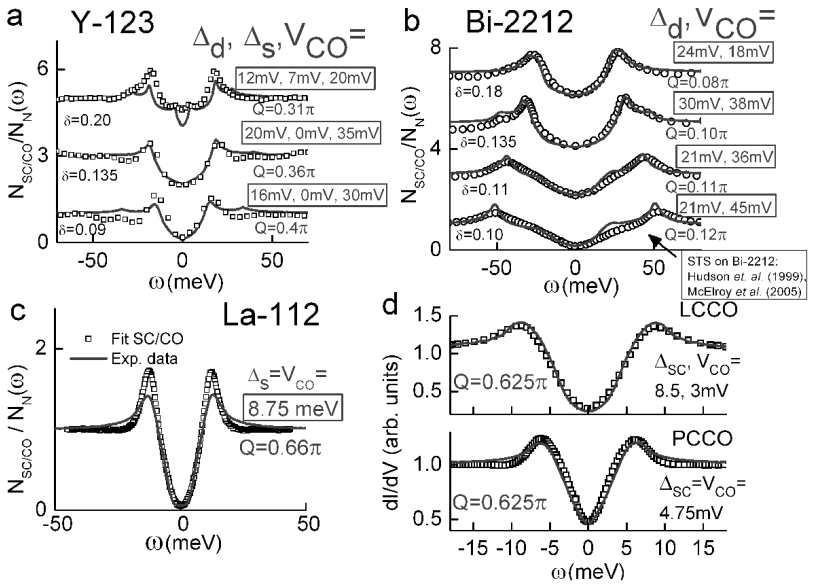

Fig. 1. (a) Comparison of normalized c-axis tunneling spectra on Y-123 of varying doping levels [28,29] (symbols) with theoretical calculations (solid lines), where the conductance of the spectra for different doping levels are slightly offset for clarity. The fitting parameters ($V_{\rm CO}$, $\Delta_{\rm SC}$) are found to be nearly independent of considering either bonding or anti-bonding bands, and the **Q**-values listed are obtained by matching the Fermi level of the antibonding band. Alternative fitting to the bonding band yields different Q-values of 0.66 π, 0.64 π and 0.61 π for $\delta = 0.09$, 0.135 and 0.20, respectively, and the fitted η value is $\sim 5 \times 10^{-7}$ for $\delta = 0.09$ and 0.135, and $\eta \sim 0$ for $\delta = 0.20$. (b) Comparison of spatially averaged c-axis tunneling spectra on Bi-2212 (symbols, from Ref. [31,32]) with theoretical calculations (solid lines). Here the Q-values are obtained by matching the Fermi level of the antibonding band, whereas consideration of the bonding band results in similar doping dependent values of ($V_{\rm CO}$, $\Delta_{\rm SC}$) but different Q-values of 0.384 π, 0.379 π, 0.366 π and 0.340 π for $\delta = 0.10$, 0.11, 0.14 and 0.18, respectively [34]. The fitted η value is $\sim 2 \times 10^{-6}$ for $\delta = 0.10$, 0.11, 0.14 and $\eta \sim 0$ for $\delta = 0.18$. (c) Comparison of a typical tunneling spectrum (open squares) [5] of electron-type optimally doped La-112 with theoretical calculations (solid line), showing $\Delta_{\rm SC} \sim V_{\rm CO}$ and $\eta \sim 5 \times 10^{-7}$, in contrast to $\Delta_{\rm SC} < V_{\rm CO}$ in optimal- and under-doped hole-type cuprates. (d) Comparison of the break-junction spectra of one-layer electron-type cuprates PCCO [4] and LCCO [35] (symbols) with theoretical calculations (solid line), showing $\Delta_{\rm SC} \sim V_{\rm CO}$ for optimally doped PCCO and $\Delta_{\rm SC} > V_{\rm CO}$ for underdoped LCCO. The fitted η value is 10^{-6} for both PCCO and LCCO.

As exemplified in Fig. 1, we compare the quasiparticle tunneling spectra taken on four different families of cuprates with the calculated DOS, where we have used different combinations of coexisting SC and CO phases based on established empirical facts: $d_{x^2-y^2}$- or $(d_{x^2-y^2}+s)$-wave SC and disorder-pinned SDW for hole-type cuprates $YBa_2Cu_3O_x$ (Y-123) [28,29] and $Bi_2Sr_2CaCu_2O_x$ (Bi-2212) [30], s-wave SC and CDW for the infinite-layer electron-type cuprate $Sr_{0.9}La_{0.1}CuO_2$ (La-112) [5], and $d_{x^2-y^2}$-wave SC and disorder-pinned SDW in one-layer electron-type cuprate superconductors $Pr_{1.85}Ce_{0.15}CuO_{4-y}$ (PCCO)

and $La_{1.884}Ce_{0.116}CuO_{4-y}$ (LCCO) [30]. In all cases, we have employed realistic bandstructures and Fermi energies for given cuprates under consideration.

The data in Fig. 1(a), represented by symbols, are our c-axis tunneling spectra on Y-123 with varying doping levels [28,29]. The c-axis tunneling data in Fig. 1(b) on $Bi_2Sr_2CaCu_2O_x$ (Bi-2212), shown as symbols for four different nominal hole-doping levels, are taken from Refs. [31,32]. In Y-123 and La-112, the quasiparticle spectra exhibit long-range spatial homogeneity so that the bulk doping level is representative of the local doping level, as manifested by the zero-field histograms of Δ_{SC} and Δ_{eff} in Figs. 2(a)-(b). In contrast to Y-123 and La-112, caution must be taken in studying the quasiparticle spectra of Bi-2212 because of the strong spatial inhomogeneity in the latter [31]. We estimate the local doping level of Bi-2212 by correlating the dominant spatially averaged spectrum of each sample with its bulk doping level, so that each empirical spectrum shown in Fig. 1(b) is spatially averaged. The data in Fig. 1(c) are taken from a representative spectrum amongst a set of momentum-independent quasiparticle tunneling spectra of the optimally doped La-112 with $T_c \approx 43$ K [5], and the data in Fig. 1(d) for optimally doped PCCO and overdoped LCCO are taken from break-junction spectra in Refs. [4,35].

To further verify the scenario of coexisting COs and SC in cuprate superconductors, we perform spatially resolved vortex-state quasiparticle spectra on two cuprates that exhibit homogeneous zero-field tunneling spectra, the optimally doped Y-123 and La-112. In conventional superconductors with SC being the only ground state, large supercurrents inside the vortex core are known to suppress SC, leading to either bound states with enhanced conductance at zero bias or flat conductance in the quasiparticle spectra [25]. In contrast, various studies of the vortex-state quasiparticle tunneling spectra of hole-type cuprate superconductors have revealed PG-like features inside the vortex core [25]. Our own investigation on Y-123 and La-112 also shows similar behavior in both hole- and electron-type cuprates, as illustrated in Figs. 2(a)-(b). Furthermore, we note that the energy scale of the PG-like features at the center of the vortex core is consistent with the V_{CO} value derived from our theoretical fitting to the zero-field experimental data, as shown in the histograms and the vortex-state conductance maps of both Y-123 and La-112 in Figs. 2(a)-(b) and also in Figs. 1(a) and (c). Hence, we suggest that the anomalous vortex-core quasiparticle spectra in cuprate superconductors can be understood in terms of a remaining CO upon the suppression of SC.

Having established the dependence of spectral characteristics on Δ_{SC} and V_{CO}, we consider next the effect of the CO wave-vector $\mathbf{Q}$ as a function of the doping level. We note that in the data fitting (solid lines) shown in Fig. 1(a)–(d), we have assumed that $\mathbf{Q}$ satisfies the nesting conditions $|\mathbf{k}+\mathbf{Q}| \sim k_F$ and $|\mathbf{k}| \sim k_F$ so that the quasiparticle excitations only occur near the Fermi mo-

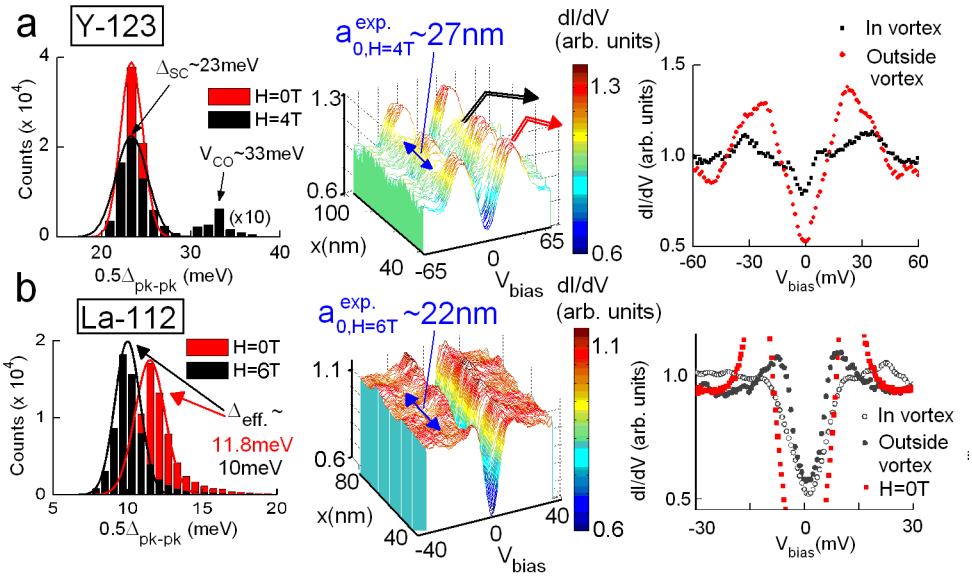

Fig. 2. (Color online) Spatially resolved quasiparticle spectra of cuprate superconductors: (a) Left panel, zero-field histogram of $\Delta_{\rm SC}$ (red or light grey) and finite-field ($H = 4$ Tesla) histogram of $\Delta_{\rm SC}$ and $V_{\rm CO}$ (dark grey) taken from an optimally doped Y-123 over an (100nm $\times$ 100nm) area at $T = 9$ K. Here the empirical gaps were taken from one-half of the peak-to-peak energy values of the tunneling spectra, so that in zero field only $\Delta_{\rm SC}$ were recorded whereas the "hump" features associated with $\Delta_{\rm eff}$ were not registered. In contrast, at $H = 4$ Tesla the empirical gap values identified from one-half of the peak-to-peak values revealed two sets of values. One of the gap values associated with the coherence peaks outside of the vortex core was found to be consistent with the zero-field $\Delta_{\rm SC}$, whereas the other associated with the PG-like features inside the vortex core was consistent with the $V_{\rm CO}$ value derived from zero-field spectral fitting. Hence, we find a homogeneous $\Delta_{\rm SC} = 23 \pm 1$ meV at $H = 0$ and a broader distribution of $\Delta_{\rm SC} = 23 \pm 2$ meV and $V_{\rm CO} = 33 \pm 2$ meV at $H = 4$ Tesla. The revelation of the CO histogram is consistent with the suppression of SC inside each vortex core and the fact that $V_{\rm CO} > \Delta_{\rm SC}$. Central panel, spatial evolution of the vortex-state quasiparticle spectra of Y-123 taken under a c-axis magnetic field $H = 4$ Tesla. The periodic spatial variations of the quasiparticle spectra are consistent with a vortex lattice constant $a_0 \sim 27$ nm. Right panel, comparison of the spectrum at the center of a vortex core with that outside of the vortex core, the former exhibit PG-like features at $V_{\rm CO} = 33 \pm 2$ meV upon the suppression of the SC coherence peaks at $\Delta_{\rm SC} = 23 \pm 2$ meV. (b) Left panel, zero-field histogram of $\Delta_{\rm eff}$ (Red or light grey) and finite-field ($H = 6$ Tesla) histogram of $\Delta_{\rm eff}$ (dark grey) taken from an optimally doped La-112 over an (100nm $\times$ 100nm) area at $T = 9$ K, showing a homogeneous $\Delta_{\rm eff} = 11.8 \pm 1.5$ meV at $H = 0$ and a downshift to $\Delta_{\rm eff} = 10 \pm 1$ meV at $H = 6$ Tesla due to the overall suppresion of $\Delta_{\rm SC}$ by magnetic field. Here we note that the c-axis upper critical field of La-112 is $H_{c2}^{c} \sim 12$ Tesla [23]. Central panel, spatial evolution of the vortex-state quasiparticle spectra of La-112 taken under a c-axis magnetic field $H = 6$ Tesla. The periodic spatial variations of the quasiparticle spectra are consistent with a vortex lattice constant $a_0 \sim 22$ nm. Right panel, quasiparticle spectrum at the center of a vortex core (black open squares) and that outside of the vortex core (black solid squares) for $H = 6$ Tesla are compared with that for $H = 0$, showing both decreasing $\Delta_{\rm eff}$ with increasing field and the revelation of PG-like features in the center of a vortex core.

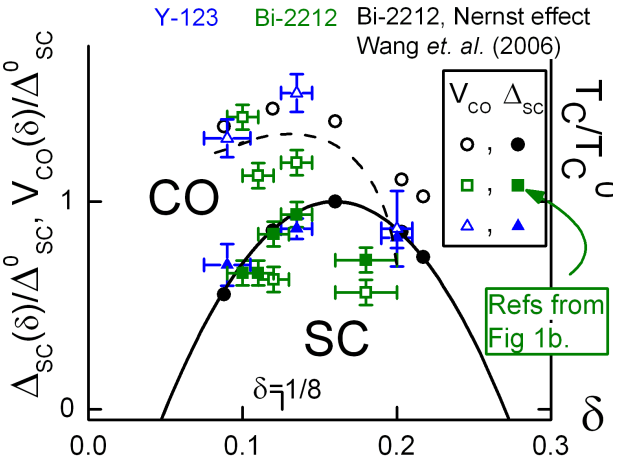

Fig. 3. (Color online) Doping dependence of $\Delta_{\rm SC}$, $V_{\rm CO}$ and T_c in hole-type cuprates Y-123 (blue or dark triangles) and Bi-2212 (green or light squares), where $\Delta_{\rm SC}$ and $V_{\rm CO}$ are normalized to their corresponding SC gaps at the optimal doping, $\Delta^0_{\rm SC}$, and T_c is normalized to the value at the optimal doping T_c^0. The doping dependent $T_{\rm onset}(\delta)$ for the onset of diamagnetism and the Nernst effect in Bi-2212 together with the corresponding $T_c(\delta)$ from Ref. [12] are shown in black circles for comparison.

mentum k_F. This assumption is justifiable for the hole-type cuprates because the degree of incommensurate spin fluctuations in these cuprates correlates with the doping level [36]. Thus, we derive the doping-dependent parameters $\Delta_{\rm SC}(\delta)$ and $V_{\rm CO}(\delta)$ for different cuprates by fitting curves to experimental data, and the parameters $\Delta_{\rm SC}(\delta)$ and $V_{\rm CO}(\delta)$ normalized to the SC gap at the optimal doping level ($\Delta^0_{\rm SC}$) of each cuprate family are summarized in Fig. 3, together with the normalized SC transition temperature (T_c/T_c^0) and the onset temperature for diamagnetism and the Nernst effect [12] ($T_{\rm onset}/T_c^0$). Our theoretical fitting to the quasiparticle DOS not only captures the primary low-energy features of the tunneling spectra in Fig. 1(a)–(d) but also yields a doping dependent $\Delta_{\rm SC}(\delta)$ that closely resembles the doping dependence of $T_c(\delta)$. In contrast, $V_{\rm CO}(\delta)$ generally increases with decreasing doping level in the doping range $0.1 < \delta < 0.22$, and the overall doping dependence also follows that of $T_{\rm onset}(\delta)$ for diamagnetism and the Nernst effect in Bi-2212 [12], as shown in Fig. 3. We further remark that the values of $\Delta_{\rm SC}$ and $V_{\rm CO}$ derived from fitting the quasiparticle DOS are insensitive to small variations in $\mathbf{Q}$, whereas ARPES characteristics are more dependent on $\mathbf{Q}$.

In addition to accounting for the primary low-energy features of doping dependent quasiparticle tunneling spectra, the notion of coexisting COs and SC can explain the spatially varying local density of states (LDOS) and the corresponding Fourier transformation of the LDOS (FT-LDOS) in Bi-2212 [21,31,33]. That is, the spatially varying LDOS may be attributed to varying parameters $(\Delta_{\rm SC}, V_{\rm CO})$ so that the LDOS $\mathcal{N}(\mathbf{r},\omega)$ is position dependent. In particular, $V_{\rm CO}(\delta)$ exhibits much stronger doping dependence than $\Delta_{\rm SC}(\delta)$, as shown in Fig. 3. Therefore, the primary cause of spatially inho-

mogeneous LDOS in Bi-2212 (in contrast to those in Y-123 and La-112) may be attributed to varying $V_{\rm CO}$ due to varying doping levels, leading to broader peaks at quasiparticle energies $\omega \sim \pm\Delta_{\rm eff}$ [13]. The spatially varying $V_{\rm CO}$ can give rise to quasiparticle scattering, yielding FT-LDOS that contains information about quasiparticle interference and the presence of CO [21].

Next, we consider the situation when the nesting condition for $\mathbf{Q}$ is relaxed. As exemplified in Fig. 4, we compare the effective gap ($\Delta_{\rm eff}$) in the first quadrant of the Brillouin zone (BZ) for s-wave SC with coexisting CDW (second row) and for $d_{x^2-y^2}$-wave SC with coexisting disorder-pinned SDW (fourth row) assuming different $\mathbf{Q}$-values, where the coupled quasiparticle states in the first BZ are illustrated above each $\Delta_{\rm eff}$ plot. For $\mathbf{Q}$ varying from $|\mathbf{Q}| < 2k_F$ (left panels), $|\mathbf{Q}| \sim 2k_F$ (middle panels), to $|\mathbf{Q}| > 2k_F$ (right panels), we find strongest CO-induced effects for $|\mathbf{Q}| \sim 2k_F$, implying maximum impact of the CO on the ground state and the low-energy excitations of the cuprates if the CO wave-vector is correlated with k_F. Interestingly, if we consider s-wave SC coexisting with a commensurate CDW ($|\mathbf{Q}| \sim 2\pi/3 > 2k_F$), the resulting $\Delta_{\rm eff}(\mathbf{k})$ becomes maximum near the "hot spots" (*i.e.*, the $\mathbf{k}$-values where the antiferromagnetic BZ and the Fermi surface intercept) of the optimally doped electron-type cuprates, as shown in the right panel of the second row in Fig. 4. This finding is analogous to the ARPES data obtained on electron-type $Pr_{0.89}LaCe_{0.11}CuO_4$ [9], where a momentum-dependent excitation potential with maximum magnitude near the hot spots is inferred and attributed to quasiparticle coupling with background antiferromagnetism (AFM). However, the existence of a long-range AFM order in zero fields or a field-induced magnetic order in the SC state of electron-type cuprates remains inconclusive [37,38]. Hence, our conjecture of s-wave SC with a commensurate CDW provides an alternative explanation for the observation in Ref. [9].

To examine the effect of DDW on the cuprates, it is informative to make comparison with the CDW case. As illustrated in Fig. 5(a), we find that in the one-band approximation the phase space associated with DDW is more restrictive so that the resulting quasiparticle spectra only exhibits PG-like features for a nearly half-filling condition (see Fig. 5(b)) [42]. If we consider the Fermi surface of a realistic hole-type cuprate [41] with a doping level deviating from half-filling, we find that due to the small phase space associated with the DDW, the DDW contributions to the quasiparticle low-energy excitations does not yield the gap-like features commonly observed in experiments, as shown in Fig. 5(c). If we take the bilayer splitting into consideration for Bi-2212 and Y-123, we find that the the anti-bonding band in Bi-2212 is comparable to the nearly nested condition, whereas neither the bonding nor antibonding band of Y-123 matches the nested condition [39]. The incompatibility of DDW with SC is also consistent with recent numerical studies of a two-leg ladder system, which reveal mutually exclusive DDW and $d_{x^2-y^2}$-wave SC states with realistic physical parameters [43].

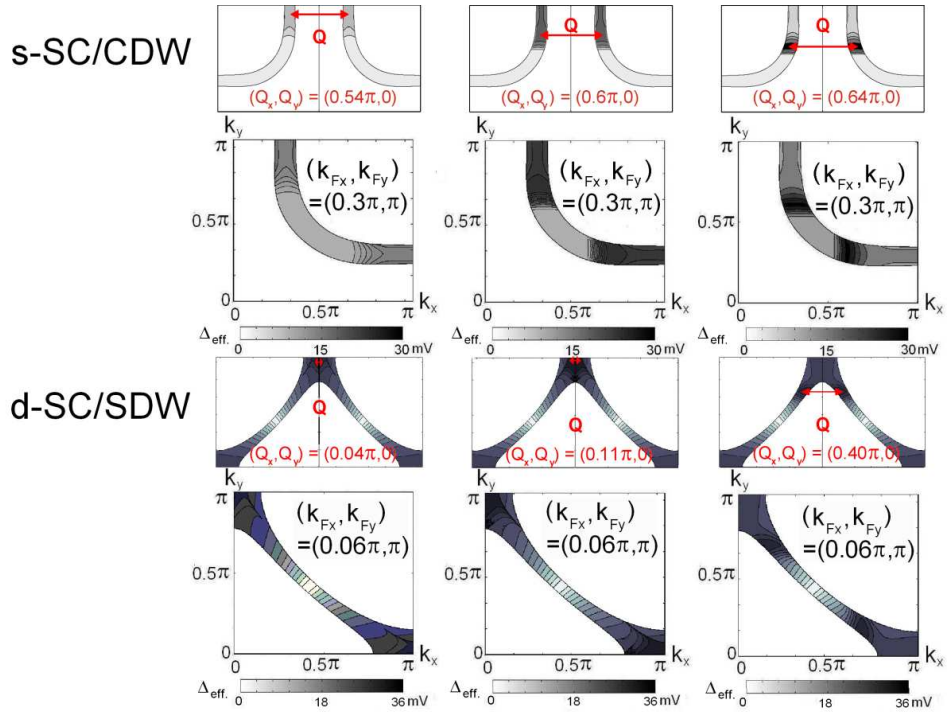

Fig. 4. (Color online) Competing order-induced dichotomy in the momentum-dependent effective gap $\Delta_{\rm eff}(\mathbf{k})$ is illustrated in the first quadrant of the BZ: The second row corresponds to the $\Delta_{\rm eff}(\mathbf{k})$ map for s-wave SC coexisting with CDW (s-SC/CDW), and the fourth row corresponds to the $\Delta_{\rm eff}(\mathbf{k})$ map for $d_{x^2-y^2}$-wave SC coexisting with SDW (d-SC/SDW). The wave-vector $\mathbf{Q}$ of the CO along either $(\pi,0)$ or $(0,\pi)$ direction varies from $|\mathbf{Q}|<2k_F$ in the left panels to $|\mathbf{Q}|\sim 2k_F$ in the middle panels and to $|\mathbf{Q}|>2k_F$ in the right panels. The phase space associated with the CDW (disorder-pinned SDW) contributions to the s-wave ($d_{x^2-y^2}$-wave) SC for different $|\mathbf{Q}|$-values is shown in the first (third) row, and the bandstructures for these calculations have included the bilayer splitting effects [39–41]. The $|\mathbf{Q}|$-values shown in the third row for the anti-bonding band correspond to twice of those of the SDW.

To further contrast the compatibility of CDW (or disorder-pinned SDW) and the incompatibility of DDW with cuprate SC, we illustrate in Fig. 5(d) comparison of the quasiparticle spectra calculated for coexisting $d_{x^2-y^2}$-wave SC and DDW (d-SC/DDW) and coexisting $d_{x^2-y^2}$-wave SC and CDW (d-SC/CDW), using the same bandstructure parameters employed in Fig. 5(c). The left panel of Fig. 5(d) corresponds to mean-field results ($\eta=0$), and the right panel corresponds to the spectra with finite quantum fluctuations $\eta=10^{-6}$. Clearly for both cases the d-SC/DDW spectra only reveal one set of peaks associated with SC, whereas the d-SC/CDW spectra can account for both the SC coherence peaks at $\pm\Delta_{\rm SC}$ and the PG features at $\pm\Delta_{\rm eff}$, suggesting that CDW (or disorder-pinned SDW) is a more likely CO than DDW for the low-energy PG phenomenon.

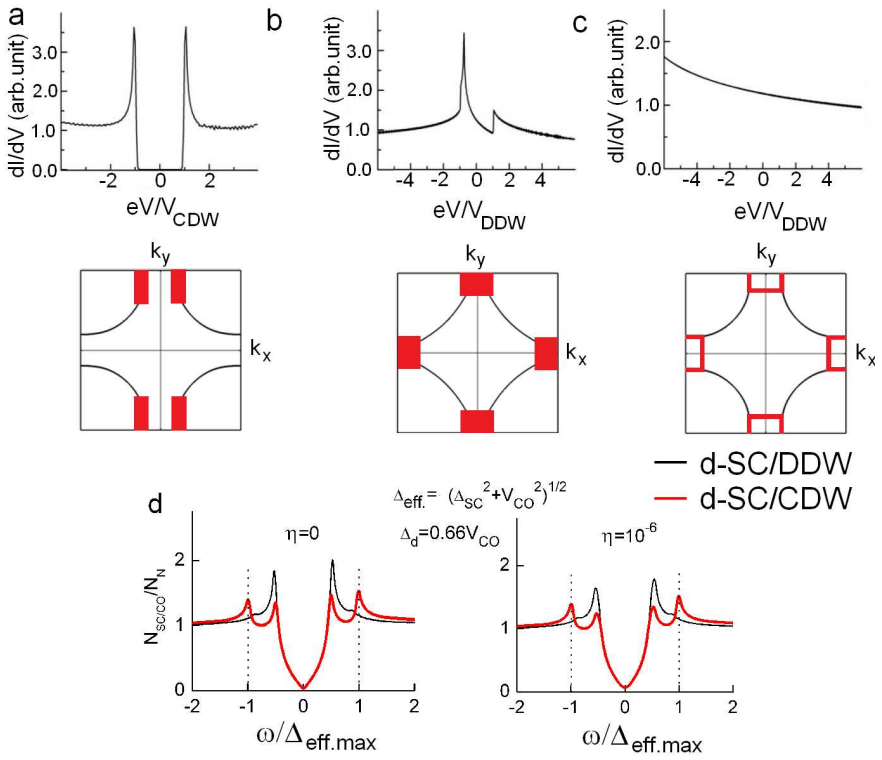

Fig. 5. (Color online) Comparison of CDW and DDW contributions to the quasiparticle excitation spectra of hole-type cuprates in the one-band approximation: (a) Quasiparticle DOS due to pure CDW in an optimally doped hole-type cuprate. The phase space associated with the CDW contributions in the first BZ is indicated (red or dark gray bars) in the lower panel. (b) Quasiparticle DOS due to pure DDW under a nearly nested condition [42]. The phase space associated with DDW in the first BZ is shown in the lower panel. (c) Quasiparticle DOS due to pure DDW in an optimally doped hole-type cuprate with realistic bandstructures [41]. The Fermi surface shown in the lower panel reveals a small phase space associated with DDW (red or dark gray lines). Here we note that related findings for the absence of gapped features in the DOS of pure DDW have also been discussed in Ref. [49]. (d) Comparison of the quasiparticle spectra calculated for coexisting $d_{x^2-y^2}$-wave superconductivity and DDW (d-SC/DDW) and coexisting $d_{x^2-y^2}$-wave superconductivity and CDW (d-SC/CDW) at $T = 0$, with the same bandstructure parameters used in (c). The left panel corresponds to mean-field results with $\eta = 0$, and the right panel corresponds to the spectra with finite quantum fluctuations $\eta = 10^{-6}$. The d-SC/DDW spectra only reveal one set of peaks associated with SC. In contrast, the d-SC/CDW spectra yield both the SC coherence peaks at $\pm\Delta_{\rm SC}$ and the satellite features at $\pm\Delta_{\rm eff}$, the latter evolving into the low-energy PG at $T > T_c$ [13].

In the context of relevant CO's for cuprate superconductors, it is worth noting a recent development that reports the onset of finite Kerr signals, albeit very small, below the PG temperature in Y-123 and in the absence of magnetic fields [44]. This finding indicates the occurrence of ferromagnetic-like signals upon the PG formation, and is compatible with broken time-reversal symme-

try. Interestingly, various CO's such as AFM, SDW, DDW and the triangular current-loop model [45] are all consistent with broken time-reversal symmetry, but are at the same time incompatible with the existence of ferromagnetism. On the other hand, local spontaneous magnetic moments solely associated with local impurity phases in Y-123 have been reported from scanning SQUID microscopy studies [46], which may give rise to weak ferromagnetic signals on average. Although the physical origin of the onset of Kerr signals below the PG temperature remains inconclusive, the aforementioned empirical and numerical information at least suggests that the DDW order parameter is unlikely the primary CO responsible for the low-energy PG in cuprate superconductors.

4 Discussion

In hole-type cuprates, additional high-energy satellite features in the quasiparticle spectra are known to exist, and the corresponding characteristic energies in Bi-2212 have been attributed to magnetic excitations [47]. Recently, evidence for phonon modes at an energy $\omega > \Delta_{\rm SC}$ and in-between the "dip" and "hump" spectral features of Bi-2212 has also been identified [48]. However, whether these high-energy bosonic modes are relevant to the occurrence of the high-energy PG remains an open issue for investigation.

If the high-energy PG is indeed associated with a bosonic energy scale $V_{\rm PG}$, we may construct a generic temperature (T) vs. doping level (δ) phase diagram of the cuprates in terms of the interplay of three primary energy scales: $V_{\rm PG}$, $V_{\rm CO}$ and $\Delta_{\rm SC}$, which correspond to temperature scales of $T_{\rm PG}(\delta)$, $T^*(\delta)$ and $T_c(\delta)$. In the case of hole-type cuprates, generally $V_{\rm CO} > \Delta_{\rm SC}$ for a wide range of doping levels, so that the CO occurs at $T^*(\delta) > T_c(\delta)$. We speculate that the larger $V_{\rm CO}$ in hole-type cuprates may be attributed to an enhanced charge transfer along the Cu-O bonding through significant coupling of the conduction carriers to the longitudinal optical (LO) phonons [50]. In contrast, no enhanced charge transfer can occur through the LO phonons in the electron-type cuprates so that $V_{\rm CO}$ is generally smaller. As a result, there is no apparent low-energy PG associated with the electron-type cuprates if $H = 0$ [4,5]. On the other hand, the higher-energy PG exists in both electron- and hole-type cuprates, which may be related to spin fluctuations and thus $V_{\rm PG} \gg \Delta_{\rm SC}$. Finally, we note that in the language of the slave-boson theory [1], $V_{\rm PG}$ may be thought of as the spinon PG in the underdoped limit. In this context, we may consider the spinon PG phase determined by the energy scale $V_{\rm PG}$ as the highly degenerate "parent phase" of all cuprates, so that AFM, SC, and CO are symmetry-breaking instabilities derived from this spin-liquid like parent phase [10].

5 Conclusion

In summary, we have investigated the low-energy excitations of cuprate superconductors in the context of coexisting COs and SC, with special emphasis on examining the effect of varying doping levels (δ) and CO wave-vectors ($\mathbf{Q}$). For various hole- and electron-type cuprate superconductors, the doping dependence of the CO energy $V_{\rm CO}(\delta)$ derived from fitting zero-field experimental tunneling spectra is consistent with the doping dependence of the low-energy PG and of the onset temperature for diamagnetism and the Nernst effect [12], which increases with decreasing δ. Moreover, $V_{\rm CO}$ values derived from the zero-field tunneling spectra of optimally doped Y-123 and La-112 are found to be consistent with the PG-like energy scales found in the center of the vortex core where SC is nearly fully suppressed. On the other hand, the SC gap $\Delta_{\rm SC}(\delta)$ derived from zero-field quasiparticle spectra is found to scale with $T_c(\delta)$, and the condition $V_{\rm CO}(\delta) > \Delta_{\rm SC}(\delta)$ holds for under- and optimal doping levels. In addition, the wave-vector $\mathbf{Q}$ of the CO in hole-type cuprates appears to be incommensurate and doping dependent, whereas the condition $V_{\rm CO}(\delta) \leq \Delta_{\rm SC}(\delta)$ is found in electron-type cuprate superconductors and the corresponding $\mathbf{Q}$ appears to be commensurate. Finally, for realistic bandstructures DDW does not couple well to the low-energy quasiparticle excitations of doped hole-type cuprates, and is therefore not a favorable CO responsible for the low-energy PG phenomena in zero fields.

References

[1] P. A. Lee, N. Nagaosa and X.-G. Wen, Rev. Mod. Phys. **78**, 17 (2006).

[2] Ch. Renner, B. Revaz, J.-Y. Genoud, K. Kadowaki, and O. Fischer, Phys. Rev. Lett. **80**, 149 (1998).

[3] T. Timusk and B. Statt, Rep. Prog. Phys. **62**, 61 (1999).

[4] S. Kleefisch, B. Welter, A. Marx, L. Alff, R. Gross and M. Naito, Phys. Rev. B **63**, 100507 (2001).

[5] C.-T. Chen, P. Seneor, N.-C. Yeh, R. P. Vasquez, L. D. Bell, C. U. Jung and S.-I. Lee, Phys. Rev. Lett. **88**, 227002 (2002).

[6] N.-C. Yeh, C.-T. Chen, V. S. Zapf, A. D. Beyer, C. R. Hughes, M.-S. Park, K.-H. Kim and S.-I. Lee, Int. J. Mod. Phys. B **19**, 285 (2005).

[7] Y. Onos, Y. Taguchi, K. Ishizaka, and Y. Tokura, Phys. Rev. Lett. **87**, 217001 (2001).

[8] J. Hwang, J. Yang, T. Timusk, S. G. Sharapov, J. P. Carbotte, D. A. Bonn, R. Liang, and W. N. Hardy, Phys. Rev. B **73**, 014508 (2006).

[9] H. Matsui, K. Terashima, T. Sato, T. Takahashi, M. Fujita, and K. Yamada, Phys. Rev. Lett. **95**, 017003 (2005).

[10] N.-C. Yeh, C.-T. Chen, A. D. Beyer, and S.-I. Lee, Chinese J. Phys. **45**, 263 (2007).

[11] Y. Wang, L. Li and N. P. Ong, Phys. Rev. B **73**, 024510 (2006).

[12] Y. Wang, N. P. Ong, Z. A. Xu, T. Kakeshita, S. Uchida, D. A. Bonn, R. Liang, and W. N. Hardy, Phys. Rev. Lett. **95**, 247002 (2005).

[13] C.-T. Chen, A. D. Beyer, and N.-C. Yeh, Solid State Comm. **143**, (Fast Communications) 447 (2007).

[14] X. J. Zhou, T. Yoshida, D.-H. Lee, W. L. Yang, V. Brouet, F. Zhou, W. X. Ti, J. W. Xiong, Z. X. Zhou, T. Sasagawa, T. Kakeshita, H. Eisaki, S. Uchida, A. Fujimori, H. Hussain, and Z.-X. Shen, Phys. Rev. Lett. **92**, 187001 (2004).

[15] S.-C. Zhang, Science **275**, 1089 (1997).

[16] S. A. Kivelson, I. P. Bindloss, E. Fradkin, V. Oganesyan, J. M. Tranquada, A. Kapitulnik, and C. Howald,Rev. Mod. Phys. **75**, 1201 (2003).

[17] J. R. Schrieffer, X. G. Wen and S. C. Zhang, Phys. Rev. B **39**, 11663 (1989) .

[18] E. Demler, S. Sachdev and Y. Zhang, Phys. Rev. Lett. **87**, 067202 (2001).

[19] A. Polkovnikov, M. Vojta, and S. Sachdev, Phys. Rev. B **65**, 220509 (R) (2002).

[20] S. Chakravarty, R. B. Lauhlin, D. K. Morr and C. Nayak, Phys. Rev. B **63**, 094503 (2001).

[21] C.-T. Chen and N.-C. Yeh, Phys. Rev. B **68**, 220505(R)(2003).

[22] H. Y. Chen and C. S. Ting, Phys. Rev. B **71**, 132505 (2005).

[23] V. S. Zapf, N.-C. Yeh, A. D. Beyer, C. R. Hughes, C. Mielke, N. Harrison, M.-S. Park, K.-H. Kim and S.-I. Lee, Phys. Rev. B **71**, 134526 (2005).

[24] A. D. Beyer, V. S. Zapf, H. Yang, F. Fabris, M. S. Park, K. H. Kim, S.-I. Lee, and N.-C. Yeh, Phys. Rev. B **76**, Rapid Communications, (2007); cond-mat/0612380.

[25] Ø. Fischer, M. Kugler, I. Maggio-Aprile, C. Berthod and Ch. Renner, Rev. Mod. Phys. **79**, 353 (2007).

[26] H.-J. Kwon and A. T. Dorsey, Phys. Rev. B **59**, 6438 (1999).

[27] H.-J. Kwon, A. T. Dorsey, and P. J. Hirschfeld, Phys. Rev. Lett. **86**, 3875 (2001).

[28] N.-C. Yeh, C.-T. Chen, G. Hammerl, J. Mannhart, A. Schmehl, C. W. Schneider, R. R. Schulz, S. Tajima, K. Yoshida, D. Garrigus, and M. Strasik, Phys. Rev. Lett. **87**, 087003 (2001).

[29] J. Y. T. Wei, N.-C. Yeh, D. F. Garrigus, and M. Strasik, Phys. Rev. Lett. **81**, 2542 (1998).

[30] C. C. Tsuei and J. R. Kirtley, Rev. Mod. Phys. **72**, 969 (2000).

[31] K. McElroy, D.-H. Lee, J. E. Hoffman, K. M. Lang, J. lee, S. Uchida, E. W. Hudson, H, Eisaki, S. Uchida, and J. C. Davis, Phys. Rev. Lett. **94**, 197005 (2005).

[32] E. W. Hudson, S. H. Pan, A. K. Gupta, K. Ng, and J. C. Davis, Science **285**, 88 (1999).

[33] J. E. Hoffman, E. W. Hudson, K. M. Lang, V. Madhavan, H. Eisaki, S. Uchida and J. C. Davis, Science **295**, 466 (2002).

[34] The doping levels listed here have been adjusted slightly from those given in Ref. [31] by better matching to the bulk T_c values.

[35] L. Alff, Y. Krockenberger, B. Welter, M. Schonecke, R. Gross, D. Manske, and M. Naito, Nature **422**, 698 (2003).

[36] B. O. Wells, Y. S. Lee, M. A. Kastner, R. J. Christianson, R. J. Birgeneau, K. Yamada, Y. Endoh, and G. Shirane, Science **277**, 1067 (1997).

[37] E. M. Motoyama, P. K. Mang, D. Petitgrand, G. Yu, O. P. Vajk, I. M. Vishik and M. Greven, Phys. Rev. Lett. **96**, 137002 (2006).

[38] P. Dai, H. J. Kang, H. A. Mook, M. Matsuura, J. W. Lynn, Y. Kurita, S. Komiya, and Y. Ando, Phys. Rev. B **71**, 100502 (2005).

[39] M. C. Schabel, C.-H. Park, A. Matsuura, Z. X. Shen, D. A. Bonn, R. Liang, and W. N. Hardy, Phys. Rev. B **57**, 6090 (1998).

[40] O. K. Andersen, A. I. Liechtenstein, O. Jepsen, and F. Paulsen, J. Phys. Chem. Solids **56**, 1573 (1995).

[41] B. W. Hoogenboom, C. Berthod, M. Peter, . Fischer, and A. A. Kordyuk, Phys. Rev. B **67**, 224502 (2003).

[42] C. Bena, S. Chakravarty, J. Hu, and C. Nayak, Phys. Rev. B **69**, 134517 (2004).

[43] U. Schollwck, S. Chakravarty, J. O. Fjrestad, J. B. Marston, and M. Troyer, Phys. Rev. Lett. **90**, 186401 (2003).

[44] J. Xia, E. Schemm, G. Deutscher, S. A. Kivelson, D. A. Bonn, W. N. Hardy, R. Liang, W. Siemons, G. Koster, M. M. Fejer, and A. Kapitulnik, arXiv:0711.2494 (2007).

[45] C. M. Varma, Phys. Rev. B **55**, 14554 (1997).

[46] E. Tafuri and J. R. Kirtley, Phys. Rev. B **62**, 13934 (2000).

[47] A. V. Chubukov, and N. Gemelke, Phys. Rev. B **61**, R6467 (2000).

[48] J. Lee, K. Fujita, K. McElroy, J. A. Slezak, M. Wang, Y. Aiura, H. Bando, M. Ishikadoand, T. Masui, J.-X. Zhu et al., Nature **442**, 546 (2006).

[49] D. Morr, Phys. Rev. Lett. **89**, 106401 (2002).

[50] M. Tachiki, M. Machida, and T. Egami, Phys. Rev. B **67**, 174506 (2003).